THE JOURNAL OF BIOLOGICAL CHEMISTRY VOL. 281, NO. 46, pp. 35186–35201, November 17, 2006

PEGylation and Multimerization of the Anti-p185^{HER-2} Single Chain Fv Fragment 4D5

EFFECTS ON TUMOR TARGETING[*] [S]

Received for publication, May 1, 2006, and in revised form, August 24, 2006 Published, JBC Papers in Press, September 8, 2006, DOI 10.1074/jbc.M604127200

Susanne Kubetzko[‡§1], **Ela Balic**[‡2], **Robert Waibel**[¶], **Uwe Zangemeister-Wittke**[‡§3], **and Andreas Plückthun**[‡4]

From the [‡]*Department of Biochemistry, University of Zürich, CH-8057 Zürich, the* [§]*Department of Oncology, University Hospital, University of Zürich, CH-8044 Zürich, and the* [¶]*Paul Scherrer Institute, CH-5232 Villigen (PSI), Switzerland*

A major goal in antibody design for cancer therapy is to tailor the pharmacokinetic properties of the molecule according to specific treatment requirements. Key parameters determining the pharmacokinetics of therapeutic antibodies are target specificity, affinity, stability, and size. Using the p185^{HER-2} (HER-2)-specific scFv 4D5 as model system, we analyzed how changes in molecular weight and valency independently affect antigen binding and tumor localization. By employing multimerization and PEGylation, four different antibody formats were generated and compared with the scFv 4D5. First, dimeric and tetrameric miniantibodies were constructed by fusion of self-associating, disulfide-linked peptides to the scFv 4D5. Second, we attached a 20-kDa PEG moiety to the monovalent scFv and to the divalent miniantibody at the respective C terminus. In all formats, serum stability and full binding reactivity of the scFv 4D5 were retained. Functional affinity, however, did change. An avidity increase was achieved by multimerization, whereas PEGylation resulted in a 5-fold decreased affinity. Nevertheless, the PEGylated monomer showed an 8.5-fold, and the PEGylated dimer even a 14.5-fold higher tumor accumulation than the corresponding scFv, 48 h post-injection, because of a significantly longer serum half-life. In comparison, the non-PEGylated bivalent and tetravalent miniantibodies showed only a moderate increase in tumor localization compared with the scFv, which correlated with the degree of multimerization. However, these non-PEGylated formats resulted in higher tumor-to-blood ratios. Both multimerization and PEGylation represent thus useful strategies to tailor the pharmacokinetic properties of therapeutic antibodies and their combined use can additively improve tumor targeting.

Antibodies have attracted attention as cancer therapeutics, because of their ability to specifically bind to cell surface antigens selectively expressed on tumor cells (1, 2). Using unarmed antibodies, fusion proteins, or chemical immunoconjugates various strategies have been investigated, which include the direct delivery of cytotoxic agents, such as radionuclides, small molecule drugs, or protein toxins (3). Moreover, indirect strategies have also been investigated, which include blocking of cellular growth factors or their receptors, recruitment of cellular or complement-dependent cytotoxicity or induction of apoptosis by receptor engagement (2, 4, 5).

Depending on the desired mode of action, the pharmacokinetic properties of the therapeutic molecule need to meet different requirements. When a cytotoxic principle is used, it is essential that the action is restricted to the tumor site as much as possible, and that the activity in normal tissues is limited both in magnitude and duration. Conversely, if the mode of action does not include a cytotoxic mechanism, accumulation in normal tissues may be less harmful, and high concentration at the tumor site can be the main criterion.

The *in vivo* behavior of the antibody format is dictated by its molecular properties. Therefore, to enhance the efficacy of therapeutic antibodies, understanding how changes of the molecular format may affect the pharmacokinetic behavior is crucial. Critical determinants of tumor targeting efficiency are specificity, affinity, valency, stability, surface charge, and size (6, 7).

In the present study, we focus on two of these parameters: functional affinity (avidity) and molecular size. Increasing the functional affinity of antibodies usually results in increased tumor localization and retention. However, there seems to be an upper limit in affinity beyond which no further improvement can be achieved (6, 8, 9): in the "loading phase", the total dose of antigen-bound antibody molecules accumulating at the tumor is limited by plasma clearance (depletion of the plasma pool) and diffusion, in addition to the total amount injected (bolus size). In the "retention phase," antigen metabolism, which includes shedding and internalization, may become rate limiting, if this occurs faster than antibody dissociation (10–12). Biodistribution studies in SCID mice with various anti-HER-2 (13) and anti-CEA[5] (14) antibodies of different affinities

* This work was supported in part by Schweizerischer Nationalfonds Grant 31-65344.01 and the Cancer League of the Kanton Zürich. The costs of publication of this article were defrayed in part by the payment of page charges. This article must therefore be hereby marked "*advertisement*" in accordance with 18 U.S.C. Section 1734 solely to indicate this fact.

[S] The on-line version of this article (available at http://www.jbc.org) contains supplementary methods.

[1] Present address: Kinderspital Zürich, Abteilung für Infektions- & Krebskrankheiten, August-Forel-Str. 1, CH-8008 Zürich, Switzerland.

[2] Present address: Inst. of Pharmacology and Toxicology, University of Zürich, CH-8057 Zürich, Switzerland.

[3] Present address: Dept. of Biochemistry, University of Zürich, CH-8057 Zürich, and Dept. of Pharmacology, University of Bern, Friedbühlstr. 49, CH-3010 Bern, Switzerland.

[4] To whom correspondence should be addressed: Dept. of Biochemistry, University of Zürich, CH-8057 Zürich, Switzerland. Tel.: 41-44-635-5570; Fax: 41-44-635-5712; E-mail: plueckthun@bioc.unizh.ch.

[5] The abbreviations used are: CEA, carcinoembryonic antigen; $^{99m}TcCO_3$, $[^{99m}Tc(OH_2)_3(CO)_3]^+$; % ID/g, percent injected dose per gram tissue; BSA, bovine serum albumin; DLS, dynamic light scattering; ECD, extracellular domain; MALS, multi-angle light scattering; NTA, nitrilotriacetic acid; PBS,

Supplemental Material can be found at:
http://www.jbc.org/cgi/content/full/M604127200/DC1

demonstrated that for a tumor antigen with the turnover rate of HER-2, raising the affinity above 10^{-9} M no longer translates into increased tumor accumulation.

One way to augment the functional affinity (avidity) of antibodies is to increase the number of binding sites (15, 16). Multivalency in principle allows the antibody to simultaneously bind to more than one target molecule on the tumor cell, provided that this is geometrically possible. By potentially affecting target dimerization, multimeric antibody formats may also increase antigen uptake and signaling. Whether this is desirable or not depends on the target and the effector mechanism of the antibody construct.

An increase in valency also results in increased molecular size, which will affect pharmacokinetics, extravasation, and diffusion, and thus tissue distribution. Indeed, there is an inverse relationship between the effect of molecular size on systemic clearance and tissue penetration, which both affect tumor targeting, albeit in opposite ways (6). Small antibody formats such as scFv fragments (25–30 kDa) show rapid tumor localization and efficient diffusion into the tumor mass, reaching maximal accumulation after 0.5–6 h. Their systemic clearance is fast and occurs mainly through renal excretion, since their molecular weight is below the threshold of the filtration barrier in the kidney glomeruli (~65 kDa) (17, 18). This results in rather low concentrations of scFv molecules in the circulation, which in turn reduces unspecific accumulation in non-target tissues, but it also reduces the total dose localizing to the tumor (19). On the other hand, large molecules, such as whole IgGs, show poor extravasation and slower tissue diffusion (20, 21). At the same time, they can exhibit prolonged serum half-lives of up to several weeks (19), because they avoid renal excretion and are instead removed by the more delayed hepatic clearance (22). The resulting high serum concentration favors accumulation in the tumor, but also unspecific localization in non-target tissues.

To define the optimal format for particular applications, various antibody formats including scFv fragments, Fab fragments, disulfide-stabilized Fv fragments (dsFv), minibodies, and miniantibodies (16) have been engineered and tested in biodistribution experiments. Although available data demonstrate that they greatly vary in tumor targeting efficiency (23–40), direct comparisons are problematic because of the great differences among the various tumor models and antigens used.

Here we systematically examined the molecular and tumor targeting properties of a series of antibody formats all derived from the same antibody fragment, as a step toward a better understanding of the relation and interdependence of these factors. As a model system, we used the humanized scFv 4D5 (24, 41). This antibody shows above-average thermodynamic and serum stability and binds selectively with high affinity to its target antigen, the extracellular domain of $p185^{HER-2}$ (35, 42) (referred to here as HER-2).

HER-2 is a 185-kDa transmembrane glycoprotein of the family of human epidermal growth factor receptors (HER) (43, 44). It is overexpressed in 20–30% of breast cancers and in a variety of other tumors of epithelial origin (45, 46). It plays a key role in HER ligand-dependent tumor growth and can either form homo- or heterodimers with other HER receptors (47).

Based on the scFv 4D5, we constructed four different antibody formats by multimerization and PEGylation, and compared their molecular and tumor targeting properties to those of the scFv 4D5 itself. First, dimeric and tetrameric miniantibodies were constructed by fusion of self-associating peptides to the C terminus of the scFv 4D5. In this approach an increase in valency was combined with a change in size from 29 kDa (monomeric scFv) to 66 kDa (dimer), which is slightly above the renal filtration threshold, and up to 130 kDa (tetramer), which is almost the size of a whole IgG. To further stabilize the multimeric formats and prevent their dissociation at high dilution, the multimerization domains were covalently linked by structure-guided introduction of disulfide bridges. In the second approach a 20-kDa polyethylene glycol moiety (PEG20) was site-specifically attached to the C terminus of the scFv 4D5. Thereby, the molecular weight of the antibody fragment was increased without altering its valency to enable us to discriminate the effects because of valency from those due to size. The PEG molecule is a non-immunogenic, hydrophilic polymer, rapidly fluctuating between bulky and extended structures (48–50). Because a PEG-tail is not a rigid moiety, but quite flexible, it can also act to shield protein sites from recognition by the immune system, cellular receptors, or proteases (51). Finally, multimerization and PEGylation were combined by site-specific PEGylation of the dimeric miniantibody.

To assess the potential of these modifications for tailoring effective antibody therapeutics, the various formats were compared regarding their antigen binding properties, serum stability, and *in vivo* biodistribution. By individually testing multimerization and PEGylation, we wished to differentiate the influence of changes in functional affinity from those of molecular size on the pharmacokinetic and tumor targeting behavior.

EXPERIMENTAL PROCEDURES

Tumor Cell Line and Recombinant Antigen—For *in vitro* cell binding experiments, as well as for tumor localization and biodistribution studies *in vivo*, the ovarian carcinoma cell line SK-OV-3 (HTB 77, ECACC, Salisbury, Wilts, UK) was used. Cell culture was performed as described (35). The purified recombinant antigen HER-2-ECD was kindly provided by Genentech Inc., South San Francisco, CA.

Molecular Modeling of the Multimerization Domains to Determine Suitable Positions for Introduction of Disulfide Bonds—The three-dimensional models of the multimerization domains were generated by using the molecular modeling software InsightII (Accelrys, San Diego, CA). The model of the dimerization domain dhlx was obtained from the average NMR structure of the corresponding synthetic peptide (52). The model of the tetramerization domain p53 was based on the crystal structure of the corresponding human peptide (53). Potential positions for insertion of disulfide bonds were determined with the program MODIP (54) using the following search parameters: allowed $C\alpha$-$C\alpha$ distance $\leq$7.4 Å, allowed $C\beta$-$C\beta$ distance $\leq$4.7 Å, pseudo bond angles in the range of 60° to 180° and disallowed pseudo-dihedral angles between 60° and

phosphate-buffered saline; PDB, Protein Data Bank; PEG, polyethylene glycol; RIA, radioimmunoassay; RU, resonance units; scFv, single chain Fv fragment; MES, 4-morpholineethanesulfonic acid.

80°. The resulting models of the multimerization domains with cross-linked peptide chains were checked for possible strain and clashes.

Construction of the Cysteine Mutants—The dimeric miniantibodies with C-terminal (4D5-dhlx-Cys) or internal cysteines (4D5-dhlx-SS) were derived from the construct 4D5-dhlx (35). The mutant 4D5-dhlx-SS with internal cysteines was generated by a two-step PCR mutagenesis of the dimerization domain, using the primer dhlx-m2 (5′-CCCCGCAAAGGCGAACTCTGCGAACTGCTGAAACATCTGAAGGAGCTGTGTAAAGGTG), which encodes point mutations that replace Glu^{23} and Ile^{33} of the dhlx domain by cysteines.

The same method was applied to obtain the tetrameric miniantibody 4D5-p53-SS. For introducing a cysteine at position Ala^{347} of the tetramerization domain we used the primer tetracys-fwd (5′-GCTGAATGAGTGCTTGGAAC) and performed PCR amplification of the vector template pIG6-4D5-p53 (35).

To enable site-specific PEGylation (55) of the monomeric scFv 4D5 (35, 41, 42, 56) and the dimeric antibody fragment 4D5-dhlx (35) with maleimide-PEG20, we added a cysteine at the C terminus of the peptide chains. For the monomeric scFv 4D5 the cysteine was introduced by PCR mutagenesis using the primer sk-cyst.rev (5′-GCATAAGCTTTCATTAACAACCACCGTGATGGTGATGGTGGTGGTTCAGGTCTTCTTCAG), which encodes a Gly_2-linker, followed by a single unpaired cysteine, 2 stop codons, and a HindIII restriction site. The dimeric miniantibody 4D5-dhlx-Cys with C-terminal cysteines was generated by ligation of the EcoRI/HindIII fragment of the plasmid pAK300-B2 into the vector pIG6-4D5 (35, 41, 42, 56). This insert was thereby placed downstream of the variable domains of the scFv 4D5 and contained the dimerization domain dhlx, followed by a His_6 tag, a Gly_4 spacer, and a cysteine. All four different antibody constructs were inserted into the expression vector pIG6 (57), like their unmodified counterparts. The correct DNA sequences of the new constructs were confirmed.

Expression and Purification—The expression and purification of the 4D5 antibody fragments are described in detail under supplementary materials. Briefly, all antibody constructs were expressed in the periplasm of the *Escherichia coli* strain SB536 (58) and purified at 4 °C by Ni-NTA chromatography and then protein A-Sepharose (because this V_H domain binds to protein A). The purified proteins were analyzed by UV-spectrometry and SDS-PAGE.

PEGylation of the 4D5 Miniantibodies—The PEGylation procedure of monomeric (scFv 4D5-Cys) and dimeric (4D5-dhlx-Cys) miniantibodies is described under supplementary materials. Briefly, purified protein samples were concentrated to ~0.3–1 mg/ml. The C-terminal cysteine residue was selectively reduced by preincubation with 3 mM dithiothreitol (final concentration) before incubation with a 5–10-fold molar excess of maleimide-PEG20 (Nektar, Huntsville, AL) for 2 h at 37 °C. The efficiency of PEGylation was analyzed by SDS-PAGE and size exclusion chromatography. The same chromatography procedure was used to purify the PEGylated proteins from both the native antibody fragments and the unreacted free PEG.

Size Exclusion Chromatography—Analytical gel filtration analysis of the multimerized and PEGylated antibody fragments was performed with an ÄKTAexplorer chromatography system (GE Healthcare, Little Chalfont, Buckinghamshire, UK) at 4 °C and a flow rate of 0.5 ml/min, using a Superdex-200 column (24-ml bed volume). The column was equilibrated with filtered and degassed phosphate-buffered saline (PBS), containing 1 M NaCl and 0.05% Tween-20. For calibration, five protein standards were used: β-amylase (β-Amyl, 200 kDa), alcohol dehydrogenase (ADH, 150 kDa), bovine serum albumin (BSA, 66 kDa), carbonic anhydrase (CA, 29 kDa) and cytochrome *c* (Cyt *c*, 12.5 kDa). The exclusion volume of this Superdex-200 column was experimentally determined as 8 ml by injection of dextran blue (~2000 kDa). Samples of the different antibody formats were injected at concentrations between 500 μg/ml and 1.2 mg/ml in a volume of 100 μl. The absorption was recorded at 280, 260, and 230 nm. If impurities or a low PEGylation yield (less than 80%) were detected, preparative size exclusion chromatography under the same conditions was used as an additional purification step.

His Tag-specific ^{99m}Tc Labeling of the Miniantibodies—The radioactive labeling of the 4D5 miniantibodies with $^{99m}Tc(CO)_3$ was performed essentially as described before (56). All constructs were rebuffered with 0.5 M MES, pH 6.5 and concentrated to ~0.7–1.3 mg/ml. In the labeling reaction they were mixed with freshly prepared $^{99m}Tc(CO)_3$ (56, 59) at a ratio of 2:1 (v/v) and incubated at 37 °C for 90 min. The degree of incorporation was checked by gel filtration analysis on a Sephadex G-25 fast desalting column (HiLoad system, GE Healthcare) connected to a HPLC radioactivity monitor (LB 508, Berthold). Unreacted free $^{99m}Tc(CO)_3$ was removed by desalting, using a Biospin-6 column (BioRAD), equilibrated with PBS. The eluted protein samples were quantified for the total amount of incorporated radioactivity by γ-scintillation counting.

Radioimmunoassay (RIA) on Human SK-OV-3 Tumor Cells—The functional affinities of the various 4D5 miniantibodies to the HER-2-overexpressing tumor cells SK-OV-3 were determined by RIA. RIAs were performed essentially as described (35), with the following modifications: stock solutions of the $^{99m}Tc(CO)_3$-labeled antibody constructs were prepared at 10 different concentrations by 2-fold serial dilution. A 20-μl aliquot of each of these stock solutions was then incubated with 100 μl of an SK-OV-3 cell suspension (corresponding to 5×10^5 cells in PBS, containing 0.5% BSA and 0.005% Tween-20) for 1 h at 4 °C on a shaker. Final concentrations of active radiolabeled miniantibodies (60) were between 0.5 nM and 1 μM. All measurements were performed in triplicates. The data obtained were fit with a 1:1 binding model, using the simplified equation $y = y_{max} \cdot x/(K_{D,\ app} + x)$, where x is the total molar concentration of radiolabeled antibody, y is the radioactivity attributable to the molecules that bound to the cells, y_{max} is its plateau value, and $K_{D,\ app}$ is the apparent equilibrium dissociation constant.

Analysis of Binding Kinetics by BIAcore Measurements—The binding kinetics of the different 4D5 miniantibody formats were analyzed and compared by surface plasmon resonance measurements using a BIAcore 3000 instrument (Biacore AB, Uppsala, Sweden). A CM5-Sepharose chip was coated by standard amine coupling chemistry (61) with the recombinant extra-

cellular domain (ECD) of the HER-2 antigen to a density of 400 RU. This rather low coating density was chosen to minimize mass transfer and rebinding effects, yet allowing residual multivalent binding to assess the functionality of the multivalent molecules. Measurements were carried out at 25 °C, using a flow rate of 30 μl/min with an association phase of 3 min after injection, followed by dissociation for 10 min. The miniantibodies were diluted in filtered and degassed HBS-EP running buffer (10 mM HEPES, pH 7.4, 150 mM NaCl, 3 mM EDTA, 0.005% Tween-20 (polyoxyethylene sorbitan monolaurate)) and injected at concentrations between 0.5 and 100 nM. For subtraction of bulk effects, caused by changes in the buffer composition or nonspecific binding, we performed double referencing (62). Therefore, all analyzed samples were additionally injected onto an uncoated reference surface, including a sample of the running buffer, which was also tested on the HER-2-coated flow cell. Data were evaluated with the BIAevaluation software (version 3.0), applying a simple 1:1 binding model. The obtained sensorgrams were fitted globally over the whole range of injected concentrations and simultaneously over the association and dissociation phase. For monomeric fragments, equilibrium dissociation constants can be calculated from the rate constants ($K_D = k_{off}/k_{on}$), whereas for multimeric fragments no true dissociation constant can be calculated; only an apparent value of the functional affinity (avidity) can be approximated for the given surface, which can still serve for relative comparisons (16).

Determination of Thermal Stability in Human Serum—The stability of the various miniantibody formats in human serum at physiological temperature was tested *in vitro*, using two different methods. In both cases the antibody fragments were radioactively labeled with $^{99m}Tc(CO)_3$ before examination. First, we determined the amount of aggregation or degradation and the stability of the functional format by size exclusion chromatography, performed on a HiLoad system (GE Healthcare). We used a Superdex-200 column (HR 10/30, 24-ml bed volume), a flow rate of 0.5 ml/min, and PBS as running buffer, containing 1 M NaCl and 0.05% Tween-20. The protein samples were injected in a volume of 100 μl. After labeling of the miniantibodies, the samples were divided into three parts. One was diluted (1:10) in human serum and incubated for 18 to 24 h at 37 °C. The other two served as controls and were diluted (1:10) in PBS buffer. Out of these one sample was loaded onto the column for immediate analysis and the other one was kept at 4 °C for the same time period as the aliquot that had been incubated in human serum. The elution profiles of the injected protein samples were recorded by simultaneous measurement of the absorption at 280 nm and the radioactivity. Because the amount of total injected radioactivity differed from sample to sample, we normalized the detected radioactivity at the main peak of each run to 1. The percentage of injected radioactivity was calculated for each elution peak, using the software Winflow (Amersham Biosciences) and Excel (Microsoft).

In the second experiment, the immunoreactive fraction of the 4D5 miniantibodies was analyzed by equilibrium binding assays on SK-OV-3 tumor cells. For all 4D5 constructs the percentage of active molecules was determined before and after incubation in human serum for 18–24 h at 37 °C. The cell binding assays were performed essentially as described (60). Triplicate samples with increasing numbers of cells (0.25 to 5×10^6 cells in 100 μl of PBS containing 0.5% BSA) were mixed with constant amounts of $^{99m}Tc(CO)_3$-labeled miniantibodies (in 20 μl of PBS containing 0.5% BSA and 0.005% Tween-20). The final concentration of miniantibody molecules in these cell suspensions was ~20 nM. The samples were incubated for 1 h at 4 °C on a shaker. Then, cells were washed three times with PBS containing 0.5% BSA and 0.005% Tween-20. The cell-bound radioactivity in the pellets was determined by γ-scintillation counting. The data obtained were fit using a 1:1 binding model.

Biodistribution Studies of the 4D5 Miniantibodies—Biodistribution studies of the various miniantibody formats were performed in mice to analyze their tumor localization, blood persistence, and body clearance. Female 6–8 weeks old CD1 nu/nu mice (Charles River, Germany) were xenografted with human SK-OV-3 tumor cells, subcutaneously injected at the lateral flanks. The studies were started 10 days after tumor inoculation, when the tumors had reached a size of 7–30 mg.

In the first experiment all 5 different 4D5 miniantibodies were compared in parallel, determining their biodistribution at 1 h and 24 h after injection. Each mouse received intravenously (i.v.) a single dose of 23 μg of $^{99m}Tc(CO)_3$-labeled antibody fragments (~100 μCi/mouse), administered in 100 μl of PBS. Mice ($n = 3$ per time point/construct) were sacrificed after 1 h and 24 h, organs were removed and the accumulated radioactivity was measured in a γ-scintillation counter. The determined radioactivity of each organ and time point was normalized to the percentage of injected dose per gram tissue (%ID/g). The total amount of injected radioactivity was arbitrarily set to 100%.

In the second biodistribution study, we focused on the PEGylated miniantibodies, using the unmodified scFv 4D5 as control. This experiment was performed essentially the same as described for the first experiment, but the change in organ distribution was followed over an extended time period. Here, mice received a single dose of 30 μg of $^{99m}Tc(CO)_3$-labeled miniantibodies each and were sacrificed at 1, 24, 48, and 66 h after injection. Because of the relatively short half-life of ^{99m}Tc (6 h), we used two different amounts of injected radioactivity, depending on the time point of the measurement. Mice, which were killed 1 h or 24 h after administration, received ~25 μCi and those sacrificed after 48 or 66 h obtained ~1 mCi.

RESULTS

Construction of Multimeric and PEGylated Miniantibodies—The functional affinity to a target antigen and the hydrodynamic size of antibody molecules are key determinants of their pharmacokinetics and tumor localization efficiency. To systematically investigate the correlation of these molecular properties with the *in vivo* behavior, we constructed and characterized four different antibody formats, all based on the anti-HER-2 scFv 4D5 (24, 41, 42), using two strategies.

First, dimeric and tetrameric miniantibody variants of the scFv 4D5 were constructed by fusion of self-associating peptides to the C terminus of the scFv fragment (35, 63). As dimerization device we used the synthetic peptide dhlx (52), consisting of a helix-turn-helix motif, which forms an interdigitating dimer. For tetramerization, the multimerization peptide of the

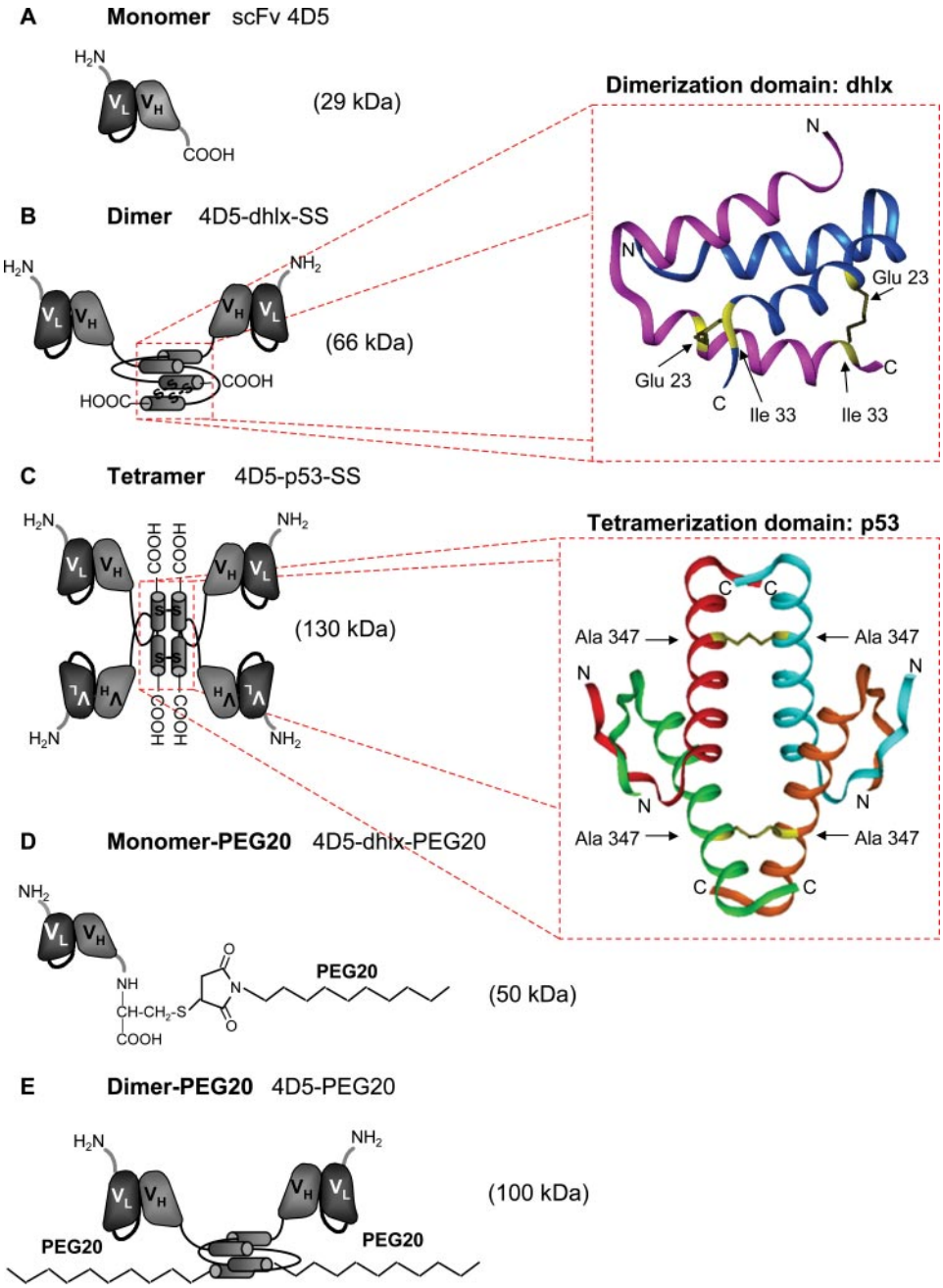

FIGURE 1. **Schematic representation of the multimerized and PEGylated 4D5 antibody fragments.** *A*, monomeric scFv 4D5 with the domain orientation V_L-V_H, connected by a non-repetitive linker (20 mer) (24, 41, 42). *B*, dimeric miniantibody 4D5-dhlx-SS. The synthetic dhlx peptide (52, 63) was fused to the C terminus of the scFv 4D5. This amphiphilic module consists of an antiparallel helix-turn-helix-motif, mediating dimerization of the fusion protein by self-association. To stabilize the dimeric format, two cysteines were introduced into the dhlx domain to achieve covalent linkage by disulfide bonds. The amino acids residues that were replaced by cysteines are depicted in *yellow* and are marked by *arrows* in the structural model of the dhlx dimerization domain. This model was obtained from the average NMR structure of the corresponding synthetic peptide (52) (PDB entry 1QP6). *C*, tetrameric miniantibody 4D5-p53-SS. For tetramerization of the scFv 4D5 the multimerization domain of the human tumor suppressor protein p53 (53) was used. The tetramer is assembled from two dimers that associate via hydrophobic interaction of α-helices and β-strands. These two subunits were covalently linked by introduction of a disulfide bridge between the pairing α-helices, as depicted in *yellow* in the structural model of the tetramerization domain p53. This model is based on the crystal structure of the corresponding human peptide (53) (PDB entry 1AIE). *D*, PEGylated scFv 4D5-PEG20. A 20-kDa polyethylene glycol moiety (PEG20) was covalently attached to a single engineered cysteine residue, introduced site-specifically at the C terminus of the scFv 4D5. The coupling was achieved by using maleimide as reactive group, forming a thioether bond with the free cysteine residue. *E*, PEGylated dimeric miniantibody 4D5-dhlx-PEG20. The same coupling method was used as for the monomeric scFv to PEGylate the dimeric antibody fragment 4D5-dhlx, resulting in a dimeric miniantibody with two PEG molecules attached.

human tumor suppressor protein p53 was chosen. The tetramer assembles from two dimers that associate via hydrophobic interactions of α-helices and β-strands (15, 31, 53). In extending our previous studies (35). we have now stabilized the multimeric formats by introducing intermolecular disulfide bonds, leading to a covalent cross-link of the self-associating peptides. To determine suitable positions for the introduction of disulfide bonds we used geometric search criteria (see "Experimental Procedures") based on structural models of the multimerization domains (Fig. 1, *B* and *C*). In the dimerization domain dhlx, two suitable positions were found, Glu^{23} and Ile^{33}, which could be replaced with cysteines (Fig. 1*B*) (numbering according to PDB file). In the tetramerization domain p53 three possible positions were determined: Phe^{328}, pairing with Phe^{338} and Ala^{347}, which is juxtaposed to the same residue of the symmetry-related peptide. Because the introduction of additional cysteines can decrease the expression yield of functional protein, which was already low in case of the tetrameric miniantibody 4D5-p53 (35), only one cysteine was introduced. To this end, we selected position Ala^{347}, which is in the middle of the associating parallel α-helices. The paired β-strands, which form an antiparallel "elbow" structure, noncovalently hold the tetramer together (Fig. 1*C*).

In a second approach, we increased the size of the scFv 4D5 by covalent attachment of a 20-kDa polyethylene glycol molecule (PEG20). The attachment site of the PEG moiety was placed at the C terminus by introducing a single unpaired cysteine residue, separated by a glycine linker from the C-terminal His_6 tag. The PEG20 polymer was coupled to the unpaired cysteine residue of the antibody fragment by an attached maleimide group, forming a thioether bond. Finally, the two

approaches were combined by adding the 20-kDa PEG-tail to the C terminus of the dimer 4D5-dhlx (35). The same coupling method was used as for the monomeric scFv, resulting in a divalent miniantibody with two PEG molecules attached. This way, a dimeric and a tetrameric miniantibody as well as a monovalent scFv with one PEG molecule attached and a bivalent miniantibody with two PEG entities were generated to be compared with the unmodified scFv (Fig. 1). The correct assembly of multimeric formats as well as the PEGylation efficiency was demonstrated by gel filtration analysis (see below).

Expression and Purification of the 4D5 Antibody Constructs—All antibody fragments were expressed in the periplasm of the *E. coli* strain SB536 (58) and purified by two subsequent affinity chromatography steps (see "Experimental Procedures" and supplementary materials). The purity of each construct was determined as greater than 90% by Coomassie-stained SDS-PAGE. After purification we routinely obtained yields of about 2–3 mg/liter *E. coli* culture of the unmodified scFv 4D5 as well as of the mutated scFv with a C-terminal cysteine, 4D5-Cys, and of the dimeric miniantibody with two cysteines in the multimerization domain, 4D5-dhlx-SS. The introduction of cysteines at these positions did not markedly decrease the expression yield. In contrast, we only obtained 500 μg/liter of the dimeric miniantibody fragment with C-terminal cysteines 4D5-dhlx-Cys under the same conditions. The yield of the tetrameric miniantibody with a disulfide bond in the tetramerization domain, 4D5-p53-SS, was only about 100 μg/l. The fact that the expression yield dropped with the introduction of additional cysteines is consistent with observations on other proteins (64–66). This is probably because of the strongly oxidizing environment in the periplasm, which may cause incorrect cross-links during folding resulting in protein precipitation (67).

Nevertheless, we chose periplasmic expression for all our constructs as the production method, since the yield was sufficient and we directly obtained active molecules (Table 3). The overall yield of active multimers was higher than by a production via inclusion bodies and refolding (data not shown). Furthermore, it should be noted that these volume yields were obtained in routine shake flasks and could potentially be greatly increased by fermentation (64).

Analysis by SDS-PAGE and Size Exclusion Chromatography—To examine whether the cysteines, introduced into the multimerization domain of the dimeric and tetrameric miniantibodies, form disulfide bonds when the antibody fragments are expressed in the periplasm of *E. coli*, we analyzed samples of the purified dimer 4D5-dhlx-SS and the tetramer 4D5-p53-SS by SDS-PAGE under reducing and non-reducing conditions (Fig. 2, *A* and *B*). Under reducing conditions both antibody fragments run according to the expected molecular size of the monomeric subunits (33 kDa). When these samples were loaded in non-reducing buffer, the protein bands shifted to about 66 kDa, which corresponds to the dimeric format. Note that in the 4D5-p53-SS design only two of the four subunits are covalently linked (Fig. 1*C*). In case of the tetrameric construct 4D5-p53-SS a faint band of the monomeric state was also detectable, indicating that a small proportion of the molecules did not properly form the disulfide bond between the multimerization domains. However, the dimeric antibody fragments as well as the main proportion of the tetrameric molecules established a covalent domain linkage under oxidizing conditions.

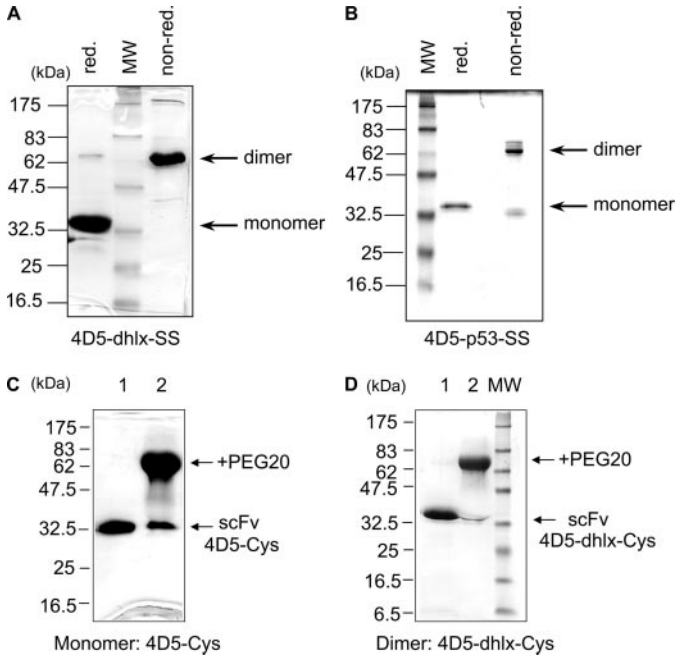

FIGURE 2. **SDS-PAGE analysis of disulfide bond formation in the multimerization domains and PEGylation of the 4D5 miniantibodies.** Purified protein samples of the different 4D5 miniantibody constructs were analyzed by 12% SDS-PAGE and stained with Coomassie Brilliant Blue. Molecular weights (*MW*) of protein standards are indicated on the *left* of each panel. To verify intermolecular disulfide bond formation in the multimerization domains of *A*, the dimeric miniantibody 4D5-dhlx-SS, and *B*, the tetrameric miniantibody 4D5-p53-SS, the apparent molecular mass of these constructs was determined under reducing and non-reducing conditions. The PEGylation yield of *C*, the monomeric scFv fragment 4D5-Cys, and *D*, the dimeric miniantibody 4D5-dhlx-Cys, was examined under reducing conditions. Samples of these constructs were analyzed before (*lane 1*) and after the PEGylation reaction (*lane 2*).

To ensure that multimerization to the expected formats of a dimeric and a tetrameric miniantibody occurred, size exclusion chromatography was performed. Purified protein samples of 4D5-dhlx-SS and 4D5-p53-SS as well as of the unmodified scFv 4D5 were analyzed on a Superdex-200 column (Fig. 3, *A*–*C*). All constructs eluted at a peak volume consistent with their expected format. In none of the protein samples were higher molecular weight aggregates detected. In the sample of the unmodified scFv 4D5 (Fig. 3*A*) a small peak at the retention volume of a dimeric antibody fragment (presumably a small amount of "diabody") (~60 kDa) was observed, in addition to the main peak of the monomeric fraction (29 kDa). The formation of this dimer was concentration-dependent, and it was stable, once formed, even if the sample was highly diluted afterward. 4D5-dhlx-SS eluted in a single symmetric peak at a retention volume consistent with the dimeric format, confirming homogeneity of the protein preparation (Fig. 3*B*). The elution peak of the tetrameric antibody fragment 4D5-p53-SS was not exactly symmetric, but had a shoulder at a retention volume of a dimeric format (Fig. 3*C*). This indicates that a small proportion of the molecules multimerized only to the dimeric stage, but the main fraction was present in a tetrameric format with a size of 130 kDa.

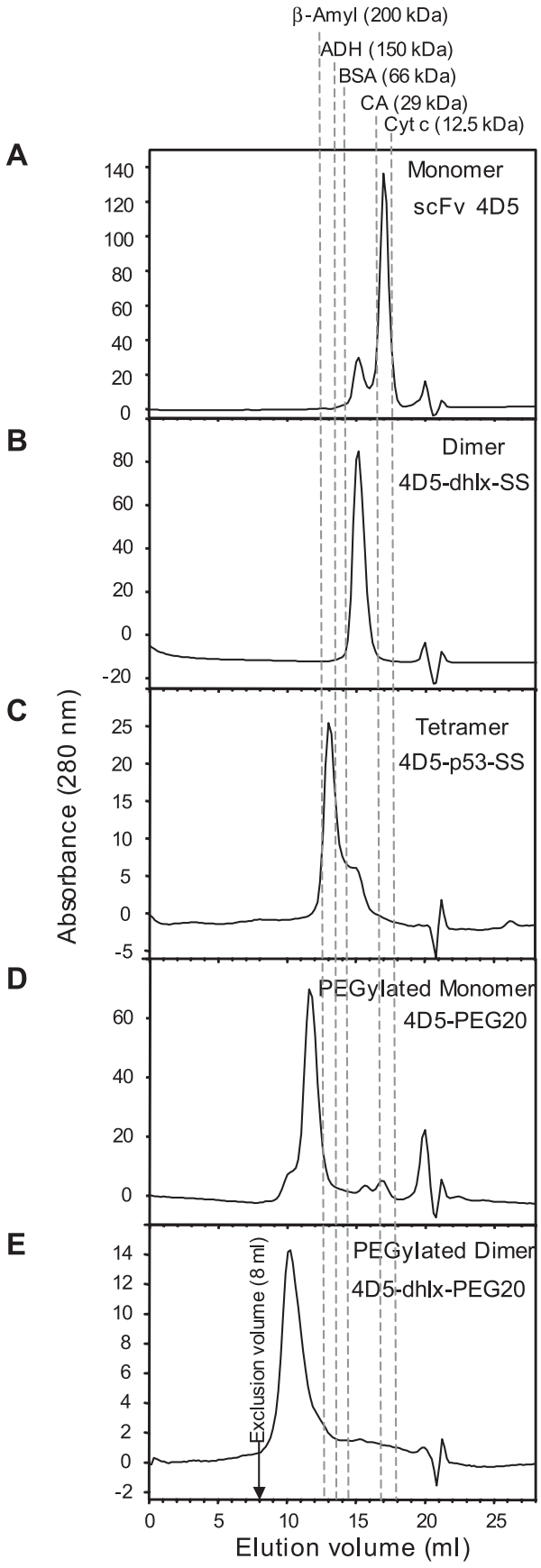

FIGURE 3. **Analysis of multimerization and PEGylation of the antibody fragments by size exclusion chromatography.** *A*, unmodified scFv 4D5 (theoretical M_r 29 kDa), *B*, dimeric miniantibody 4D5-dhlx-SS (66 kDa), *C*, tetrameric miniantibody 4D5-p53-SS (132 kDa), *D*, PEGylated scFv 4D5-PEG20 (50 kDa), and *E*, PEGylated dimeric miniantibody 4D5-dhlx-PEG20 (106 kDa) were analyzed on an ÄKTA system with a Superdex-200 column (24-ml bed-volume). Molecular mass standards: β-amylase (M_r 200 kDa, elution volume 12.67 ml), alcohol dehydrogenase (M_r 150 kDa, elution volume 13.47 ml), bovine serum albumin (M_r 66, kDa, elution volume 14.3 ml), carbonic anhydrase (M_r 29 kDa, elution volume 16.62 ml), and cytochrome *c* (M_r 12.5 kDa, elution volume 17.7 ml). The elution volumes of the antibody fragments were 17.0 ml (scFv 4D5), 15.09 ml (4D5-dhlx-SS), 13.03 ml (4D5-p53-SS), 11.88 ml (4D5-PEG20), and 10.15 ml (4D5-dhlx-PEG20). In none of the protein samples were higher molecular weight aggregates detected at the exclusion volume (8 ml).

SDS-PAGE and gel filtration analysis were also used to control for the PEGylation yield of the monomeric and dimeric miniantibodies with C-terminal cysteines. First, we compared the migration behavior of the purified antibody fragments before and after PEGylation on a 12% SDS-gel under reducing conditions. We found a band shift upon PEGylation, increasing the apparent molecular weight of the antibody fragments from 32 kDa (monomeric state) to about 62 kDa (Fig. 2, *C* and *D*). Only a small fraction of the proteins did not react with PEG20 and thus appeared as faint band at the same size as the untreated sample. Therefore, the PEG20 moiety could be shown to be attached to the monomeric as well as to the dimeric miniantibody with a conjugation yield of ~80–90%. Because the dimeric miniantibody gave rise to only one main band in the denaturing SDS-PAGE, corresponding to the PEGylated form, a major fraction of these dimers must have two PEG20 molecules attached, one on each subunit. The retention of the internal disulfide bonds in the V_L and V_H domains under the PEGylation conditions applied was verified by subjecting the unmodified scFv 4D5 to the same reaction procedure as described above. In this case, no attachment of the PEG polymer to the protein could be detected (data not shown).

In the gel filtration analysis, both PEGylated miniantibody constructs eluted as symmetric peaks without showing high molecular weight aggregates and only a minor fraction of non-PEGylated molecules (Fig. 3, *D* and *E*). The small height of these minor peaks in comparison to the main peak of PEGylated proteins is in agreement with the high PEGylation yield determined in the SDS-PAGE analysis. As observed for the unmodified monomeric scFv 4D5, the scFv 4D5-PEG20 also appears to dimerize to a small extent when it is highly concentrated. The elution peak of the PEGylated monomer had a small shoulder at the same retention volume as the PEGylated dimer 4D5-dhlx-PEG20.

When comparing the behavior of the PEGylated proteins with that of the non-conjugated antibody fragments by gel filtration, it became apparent that the PEGylated constructs eluted at a retention volume corresponding to a size of 200–300 kDa, which is not consistent with the calculated molecular weight (50 kDa for the monomer-PEG20 and 106 kDa for the dimer-PEG20). We could confirm the theoretical molecular mass of about 50 kDa at least for the monomer-PEG20 construct by multi-angle static light scattering (MALS), performed online during the gel filtration runs (55). This behavior of PEG in gel filtration is in agreement with the findings of other groups (49, 50, 68, 69). It demonstrates the strong effect of the 20-kDa PEG-tail on the diffusion behavior of the conjugated protein,

TABLE 1

Functional affinity of 4D5 miniantibodies on SK-OV-3 cells

Binding interaction of the ^{99m}Tc-labeled antibody fragments with the p185^{HER-2} overexpressing tumor cells SK-OV-3 was measured in a RIA format at 4 °C (see "Experimental Procedures"). Apparent functional affinities were calculated from the fit of the data, using the simplified equation $y = y_{max} \cdot x/(K_{D,\ app} + x)$, where y is proportional to the number of bound antibody molecules and x is their total molar concentration and y_{max} is the plateau value. We thus assumed a simple 1:1 binding model, even though only the monomeric antibody fragments are properly described by this model.

Antibody fragment	Functional affinity on SK-OV-3 cells
	nM
Monomer: scFv 4D5	29.3 ± 5.15
Dimer: 4D5-dhlx-SS	11.9 ± 1.04
Tetramer: 4D5-p53-SS	10.2 ± 1.9
PEGylated monomer: 4D5-PEG20	138 ± 37.2
PEGylated dimer: 4D5-dhlx-PEG20	67 ± 6.80

TABLE 2

Binding kinetics of the 4D5 miniantibodies

Association and dissociation kinetics of the various constructs were compared by surface plasmon resonance measurements. A CM5-Sepharose chip was coated with p185^{HER-2} (HER-2)-ECD antigen to a density of 400 RU. The miniantibodies were injected at a high flow rate of 30 μl/min, using concentrations between 0.5 nM and 100 nM. Data were evaluated with BIAevaluation 3.0 software, applying a 1:1 binding model and a global fit. This was possible because of the very slow off-rates, resulting in global fits of similar quality. Nevertheless, this gives a K_D value only for the monomeric construct; for the multivalent ones only apparent functional affinities (avidities) can be deduced, which can be used for relative comparisons only.

Construct	k_{on}	k_{off}	$K_{D,\ app}$	χ^2
	$M^{-1}\ s^{-1}$	s^{-1}	M	
Monomer	$3.4 \cdot 10^5$	$5.0 \cdot 10^{-5}$	$1.5 \cdot 10^{-10}$	0.7
Monomer-PEG20	$6.1 \cdot 10^4$	$4.9 \cdot 10^{-5}$	$8.1 \cdot 10^{-10}$	0.6
Dimer	$9.8 \cdot 10^5$	$2.6 \cdot 10^{-5}$	$2.6 \cdot 10^{-11}$	4.2
Dimer-PEG20	$2.7 \cdot 10^5$	$3.5 \cdot 10^{-5}$	$1.3 \cdot 10^{-10}$	1.9
Tetramer	$6.5 \cdot 10^5$	$8.7 \cdot 10^{-5}$	$1.3 \cdot 10^{-10}$	0.2

enlarging its hydrodynamic radius far beyond that expected from the increase in molecular weight.

To verify this conclusion and to exclude any interference of the column material, we also examined the different antibody formats in solution by dynamic light scattering (DLS). Based on the diffusion coefficients determined (55), the apparent molecular weights of the constructs, when treated as globular proteins, were calculated. The diffusion coefficients of the PEGylated antibody fragments corresponded to sizes of 133 and 309 kDa, respectively. These values are clearly above their actual molecular mass and consistent with the results of the gel filtration analysis.

RIA Measurements of Functional Affinities on SK-OV-3 Tumor Cells—Multimerization and PEGylation are modifications, which can affect the functional affinity of antibodies to cell surface antigens. By multimerization, the valency of the antibody fragment is increased, in principle allowing it to bind to more than one antigen molecule simultaneously. By attachment of a 20-kDa polyethylene glycol moiety, a highly flexible, bulky residue with a long reach was added to the protein. This PEG-tail can dynamically interfere with the antigen-antibody binding interaction, and in addition, upon binding, block the binding to a neighboring antigen (55).

To analyze if and to what degree the functional affinities of the 4D5 miniantibodies were altered by these modifications, we performed equilibrium binding measurements on HER-2-overexpressing SK-OV-3 tumor cells by RIA. As a reference molecule, the unmodified scFv 4D5 was used. For all constructs we determined functional affinities in the nanomolar range (Table 1). This is in agreement with earlier results of RIA measurements, which were performed with our first generation of 4D5-miniantibodies, lacking the disulfide bridges between the multimerization domains (35). As expected, we found an increase in functional affinity for the di- and tetrameric miniantibodies 4D5-dhlx-SS and 4D5-p53-SS in comparison to the monomeric scFv fragment.

In contrast, both PEGylated constructs showed decreased functional affinities of about 4–6-fold, compared with the respective non-PEGylated molecule. Thus, PEGylation significantly reduced the apparent affinity of the 4D5 antibody fragments, although the PEG20 moiety was attached site-specifically at the C terminus of the proteins, and thus most distal to the antigen binding site.

Comparison of Binding Kinetics by Surface Plasmon Resonance—To investigate the effect of multimerization and PEGylation on the apparent affinity of the 4D5 antibody fragments in more depth, we compared the binding kinetics of the five different antibody constructs by surface plasmon resonance. The association and dissociation rates were separately analyzed using a BIAcore 3000 instrument. The antigen was coated on a CM5 chip at a density of 400 RU. This coating density was chosen because it is relatively low, allowing to minimize mass transport effects and rebinding of fully dissociated molecules, which both could compromise the measured kinetics. On the other hand, this coating density is still sufficient to enable some multivalent binding, required to verify the functionality of the multivalent constructs. Measurements were performed at a high flow rate of 30 μl/min to minimize rebinding, using analyte concentrations from 0.5 to 100 nM. The k_{on}, k_{off}, and apparent K_D values determined are listed in Table 2. It is important to note that these values can only be used for relative comparisons, as they have been approximated from a 1:1 model, which only holds true for the monovalent species. For the multivalent species only apparent values of functional affinities or avidities (valid for the particular immobilization density used) can be deduced. However, because of the very slow dissociation rate, deviations from a 1:1 model are not apparent from the quality of the fit of the multivalent species (55).

For the non-PEGylated constructs we determined functional affinities in the picomolar range. This is in agreement with earlier results (42) and with the functional affinities determined for the monoclonal antibody humAb4D5–8 (24) and the 4D5 Fab fragment (70). In all of these measurements the soluble recombinant HER-2-ECD was used, whereas the RIA experiments were performed on whole cells. Thus, the discrepancy between the determined apparent K_D values, when comparing the BIAcore with the RIA data (Tables 1 and 2), is probably because of partial inaccessibility of the epitope recognized on cell-bound HER-2 (44). As this difference is also observed for the monomeric species, this is unlikely to be linked to epitope density.

For the PEGylated constructs we determined apparent K_D values of 800 pM (monomeric scFv 4D5-PEG20), and 130 pM (bivalent dimer 4D5-dhlx-PEG20). These values indicate each about a 5-fold lower functional affinity than the corresponding constructs without a PEG-tail, measured on the same surface. Separate analysis of the association and dissociation kinetics

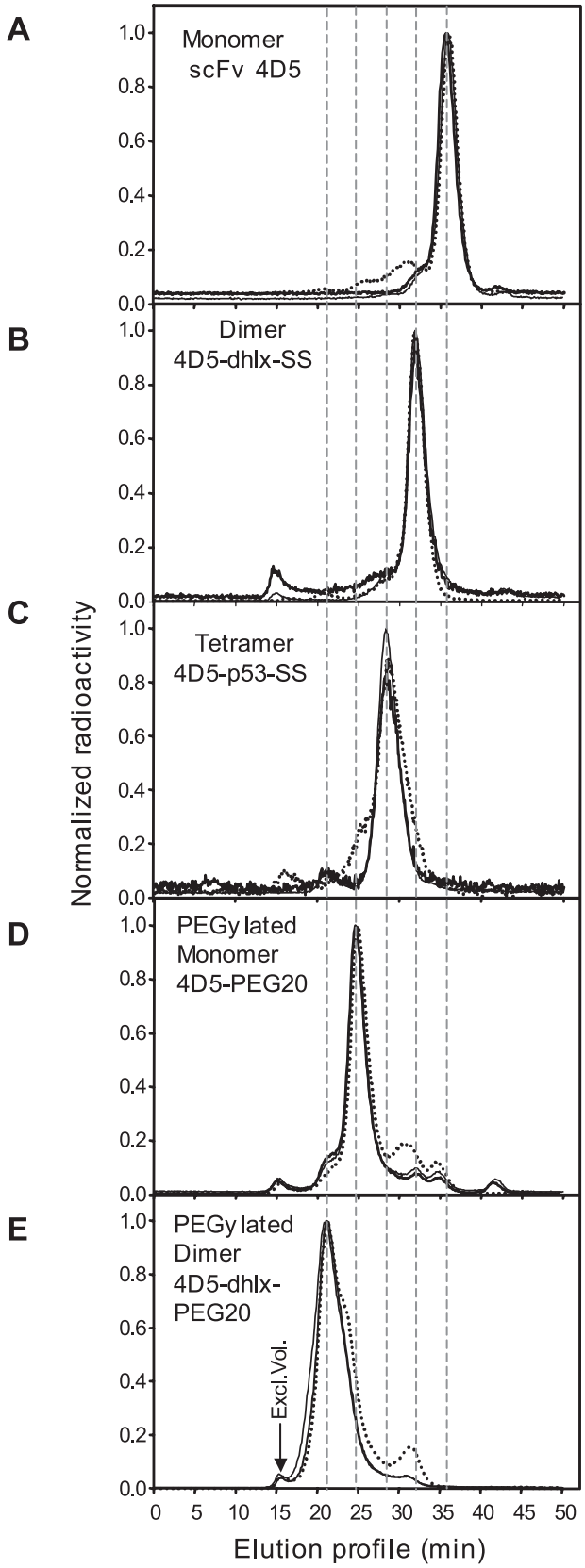

FIGURE 4. **Thermal stability of the 4D5-derived miniantibodies in human serum, analyzed by size exclusion chromatography.** The 4D5 miniantibodies were radioactively labeled with $^{99m}Tc(CO)_3$ and incubated in human serum for 18–24 h at 37 °C and in parallel also in PBS at 4 °C for the same time period as a reference. The integrity of the different formats was controlled by size exclusion chromatography on a Superdex-200 column before (*thick solid line*) and after incubation in human serum (*dashed line*) or PBS (thin *solid line*). To be able to compare the proportion of aggregates or degradation products in relation to the amount of molecules in their functional format, the radioactivity measured at the peak of the elution profile of each protein sample was normalized to 1. The corresponding retention time of each miniantibody format is indicated by a *vertical line*. *A*, monomeric scFv 4D5 (29 kDa); *B*, dimeric miniantibody 4D5-dhlx-SS (66 kDa); *C*, tetrameric miniantibody 4D5-p53-SS (132 kDa); *D*, PEGylated scFv 4D5-PEG20 (50 kDa, theoretical M_r); and *E*, PEGylated dimeric miniantibody 4D5-dhlx-PEG20 (106 kDa theoretical M_r).

revealed that the reduction in functional affinity, caused by PEGylation of the antibody fragments, was due almost exclusively to a slower on-rate (Table 2), while the off-rate remained essentially unchanged.

To exclude a difference in the percentage of functional molecules as a possible cause for reduced affinity upon PEGylation, we evaluated the fraction of active molecules in the injected protein samples by a second set of BIAcore measurements performed under mass transport limitations (55). We determined a fraction of 90–100% active molecules for all constructs, with no significant difference between PEGylated and unconjugated miniantibodies. This is consistent with the fraction of active molecules determined on whole cells (see below).

Thermal Stability in Human Serum—A prerequisite for efficient tumor localization of antibodies is their high stability in serum at physiological temperature. To address this issue we examined the stability of the different 4D5 miniantibody formats upon incubation in human serum at 37 °C and measured their aggregation and degradation behavior as well as their antigen binding activity. For this purpose, the antibody constructs were labeled with $^{99m}Tc(CO)_3$ and analyzed before and after serum incubation for 18–24 h by size exclusion chromatography and binding assays on HER-2 overexpressing tumor cells.

In the gel filtration analysis the elution profiles of freshly labeled miniantibodies were compared with aliquots that had been incubated in serum at 37 °C or in PBS at 4 °C (Fig. 4). For all five constructs we found that the main portion of injected molecules still eluted at the same peak volume after serum incubation as observed before this treatment. Only in case of the monomeric scFv 4D5 and the tetramer 4D5-p53-SS a small fraction of oligomerized or aggregated molecules was detected after serum incubation. The elution profiles of the PEGylated constructs showed, in addition to their main elution peak, small peaks at about the same retention time (30–35 min) as the non-PEGylated scFv fragments. However, we do not know the true identity of these minor peaks, and they may contain some material which was never PEGylated or might have resulted from minor proteolytic activity in the sample. The percentage of molecules that retained their initial format upon serum incubation at 37 °C for 24 h was determined as 65% for the monomer, 85% for the dimer, 48% for the tetramer, 66% for the PEGylated monomer and 81% for the PEGylated dimer. Overall, the elution profiles obtained indicate that each of the different antibody formats has sufficient stability in human serum at 37 °C for at least 24 h.

To determine the immunoreactivity of the 4D5 miniantibodies on SK-OV-3 tumor cells before and after serum incubation, cell binding assays with increasing numbers of cells were per-

formed (60). Only a small decrease in binding activity (by 0–20%) was found over time for all constructs. Combining the initial percentage of active molecules with this decline, a remaining fraction of 69–91% immunoreactive antibody molecules (Table 3) were obtained after serum incubation. This finding supports the conclusion that the high serum stability of the 4D5 scFv could be retained in the multimerized and PEGylated formats.

Blood Clearance and Tumor Localization—The different miniantibody formats were generated to investigate the effects of changes in size and functional affinity on systemic clearance and tumor localization. Biodistribution studies were performed in mice bearing subcutaneously growing SK-OV-3 tumor xenografts.

In a first experiment, all five different constructs were compared in parallel by measuring their biodistribution 1 h and 24 h after injection (Table 4 and Fig. 5). The first aim of this experiment was to clarify whether the insertion of disulfide bonds into the multimerization domains of the dimeric and tetrameric antibody fragments would influence *in vivo* stability, compared with the constructs without a covalent bond (35). The second aim was to assess the effect of PEGylation on serum half-life and tissue distribution. The unmodified monomeric scFv 4D5 localized at the tumor site with 1.77% ID/g and a tumor-to-blood ratio of 9.3 after 24 h. These data are in the same range as those reported in previous targeting studies using this scFv in the same tumor model (35, 56). For the dimeric miniantibody 4D5-dhlx-SS we measured a tumor accumulation of 2.1% ID/g with a tumor-to-blood ratio of 7.8, 24 h after injection. At this time point, the tetrameric miniantibody 4D5-p53-SS showed a tumor localization of 2.84% ID/g and a tumor-to-blood ratio of 3.84. When comparing the total dose accumulation of these three miniantibodies, we found a moderate increase in tumor localization with increasing degree of multimerization. These data are qualitatively and quantitatively consistent with the results of a previous targeting study, performed with dimeric and tetrameric antibody fragments of the same format but lacking disulfide bonds in their multimerization domains (35). The covalent linkage of the multimerization domains neither improved the tumor accumulation of the miniantibodies nor did it alter their blood clearance. Therefore, the fact that tumor enrichment of these multimeric miniantibodies remains relatively modest, despite their high functional affinity, cannot be explained by partial dissociation of their subunits.

Attachment of the 20-kDa PEG moiety, however, significantly altered the targeting properties of the antibody fragments. The PEGylated constructs accumulated at the tumor site with 9.5% ID/g (monomer-PEG20) and 11.6% ID/g (dimer-PEG20) 24 h after injection, showing tumor-to-blood ratios of 3 (monomer-PEG20) and 1 (dimer-PEG20). PEGylation of the antibody fragments thus strongly increased their serum half-life, thereby leading to higher tumor accumulation, but also to decreased tumor-to-blood ratios. In comparison, the multimeric miniantibodies without PEG-tail did not achieve the same level of tumor accumulation, but conversely showed higher tumor-to-blood ratios.

Because the blood concentration of the PEGylated antibody fragments was still high after 24 h, especially in case of the dimer 4D5-dhlx-PEG20, we decided to perform a second extended biodistribution study. Here, we analyzed the change in organ distribution of the PEGylated molecules over time by taking blood, tumor and organ samples 1, 24, 48, and 66 h after injection (Table 5 and Fig. 6). Unmodified scFv 4D5 was used as reference. The PEGylated monomer reached its highest tumor accumulation between 24 and 48 h after injection with 9.28% ID/g (24 h) and 8.74% ID/g (48 h). After 66 h still 4.85% ID/g were present at the tumor with a tumor-to-blood ratio of 10.3, indicating stable antigen binding and retention in the tumor tissue. At 24 h after injection the PEGylated dimer still had a tumor-to-blood ratio of 1 and a total dose enrichment comparable to the monomer-PEG20. It reached its highest tumor accumulation not before 48 h after injection, showing 15% ID/g with a tumor-to-blood ratio of 2.53. However, after 66 h only

TABLE 3

Immunoreactivity of the 4D5 miniantibodies on SK-OV-3 cells before and after serum incubation

The ^{99m}Tc-labeled miniantibodies were incubated in human serum for 18–24 h at 37 °C. The percentage of active molecules was determined for each construct before and after serum incubation by equilibrium binding assays on SK-OV-3 cells as described (60). The data were fit using a 1:1 binding model.

Antibody fragment	Immunoreactive fraction on cells[a]	
	Before serum incubation	After serum incubation
	%	%
Monomer: scFv 4D5	94	71
Dimer: 4D5-dhlx-SS	89	79
Tetramer: 4D5-p53-SS	80	69
PEGylated monomer: 4D5-PEG20	90	91
PEGylated dimer: 4D5-dhlx-PEG20	85	70

[a] Immunoreactive fraction means binding to the p185^{HER-2} antigen with at least one binding site.

TABLE 4

Biodistribution of the ^{99m}Tc-labeled 4D5 miniantibodies in nude mice bearing SK-OV-3 tumor xenografts 24 h after injection

The first *in vivo* study, comparing the biodistributions of the 5 different constructs in parallel at 1 h (not shown) and 24 h post-injection, was carried out in nude mice bearing SK-OV-3 xenografts. Here, only the organ distributions 24 h after injection are given as the mean % ID/g tissue ± S.D.

Organ	Monomer[a]	Dimer	Tetramer	Monomer-PEG20	Dimer-PEG20
Heart	0.3 ± 0.04	1.5 ± 0.25	1.0 ± 0.13	2.35 ± 0.37	6.76 ± 1.71
Spleen	0.82 ± 0.19	8.2 ± 3.5	5.7 ± 0.33	2.65 ± 0.49	7.2 ± 2.73
Liver	2.6 ± 0.3	9.5 ± 2.1	13.8 ± 1.2	4.63 ± 0.78	11.9 ± 0.28
Kidney	105 ± 24	107 ± 29	66.6 ± 42	97.8 ± 12	72.3 ± 32
Stomach	0.9 ± 1	1.1 ± 0.9	0.67 ± 0.24	1.2 ± 0.78	1.6 ± 0.39
Blood	0.19 ± 0.01	0.27 ± 0.02	0.74 ± 0.13	3.15 ± 2.38	12.4 ± 1.9
Tumor	1.77 ± 0.23	2.1 ± 0.48	2.84 ± 0.85	9.5 ± 0.21	11.6 ± 1.56
Tumor/blood[b]	9.3	7.8	3.84	3.0	0.94

[a] The constructs refer to Fig. 1.
[b] The ratios represent the average of the tumor/blood values for the individual mice ($n = 3$) and were calculated from non-rounded values, while the numbers in the table have been rounded.

5.2% ID/g were still retained in the tumor tissue, which is almost equivalent to the value of the monomer-PEG20 at this time point. Compared with the unmodified scFv 4D5, both PEGylated constructs achieved a distinctly increased tumor enrichment of 5.5-fold (24 h after injection). After 48 h, the difference was even stronger with an 8.5-fold (monomer-PEG20) and 14-fold (dimer-PEG20) higher tumor accumulation, respectively, compared with the scFv.

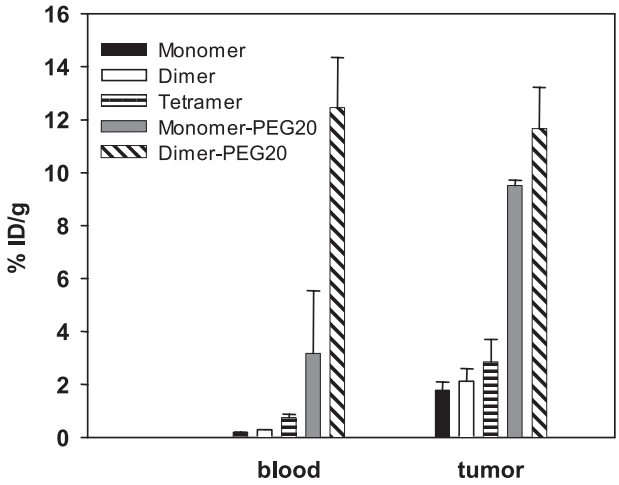

FIGURE 5. **Serum persistence and tumor accumulation of the 4D5 miniantibodies in mice.** Miniantibodies were radioactively labeled with $^{99m}Tc(CO)_3$ and injected into nude mice bearing SK-OV-3 carcinoma xenografts. Each mouse received a protein sample of 23 μg intravenously. Mice (n = 3 per time point) were sacrificed after 1 h and 24 h, organs were taken and measured for incorporated radioactivity. The determined radioactivity of each organ was normalized to the percentage of injected dose per gram tissue (% ID/g). In this bar graph only the blood and tumor values 24 h after injection are shown. The complete list of organ values is given in Table 4.

In summary, among the 5 tested formats the PEGylated dimeric miniantibodies showed the most favorable tumor targeting properties regarding overall total dose enrichment. On the other hand, the PEGylated monomer and the unconjugated miniantibodies showed higher tumor-to-blood ratios and faster clearance from normal non-target tissues.

DISCUSSION

To facilitate the development of improved tumor targeting strategies, we investigated how and to what extent modifications in size and affinity can alter the pharmacokinetic and tumor targeting properties of recombinant antibody fragments. To this end, we generated and compared four different antibody formats all derived from the scFv hu-4D5 (24, 41). This scFv was chosen because of its favorable biophysical properties, which enabled us to analyze the effects of the molecular modifications without functional limitations by the parental scFv itself. The different antibody formats were generated by either multimerization or PEGylation or by combining both modifications.

Molecular Design—In the first approach, dimeric and tetrameric miniantibody variants of the 4D5 scFv were generated by fusion of self-associating peptides to the C terminus of the antibody fragment (35). This enabled the spontaneous assembly of the subunits already during their expression, directly in the periplasm of *E. coli*. To further stabilize the multimeric formats, in an extension of our previous studies (35), we now intro-

TABLE 5

Biodistribution of the scFv, PEGylated scFv, and PEGylated dimeric miniantibodies in nude mice bearing SK-OV-3 tumor xenografts

Biodistributions of the scFv 4D5 (monomer) as well as of the PEGylated scFv (monomer-PEG20) and the PEGylated dimeric antibody fragment (dimer-PEG20) were analyzed in nude mice, xenografted with human SK-OV-3 tumors. Mice (n = 3 per time point) were sacrificed and organs excised at 1, 24, 48, and 66 h after injection of the $^{99m}Tc(CO)_3$-labeled constructs. Data are given as percentage of injected dose per gram tissue (% ID/g) and expressed as the mean ± S.D.

Construct	Organ	1 h	24 h	48 h	66 h
Monomer	Heart	1.63 ± 0.12	0.48 ± 0.05	0.34 ± 0.04	0.27 ± 0.11
	Spleen	1.83 ± 0.33	1.84 ± 0.39	0.76 ± 0.27	0.62 ± 0.17
	Kidney	204.5 ± 9.5	125.6 ± 13.6	77.8 ± 11.8	68.3 ± 21.4
	Liver	2.84 ± 0.22	2.69 ± 0.5	1.80 ± 0.29	1.11 ± 0.21
	Stomach	0.50 ± 0.03	0.40 ± 0.09	0.33 ± 0.15	0.15 ± 0.05
	Intestine	0.81 ± 0.08	0.40 ± 0.10	0.25 ± 0.09	0.18 ± 0.02
	Bone	0.83 ± 0.11	0.39 ± 0.13	0.24 ± 0.05	n.d.[a]
	Blood	2.69 ± 0.08	0.19 ± 0.03	0.1 ± 0.01	0.07 ± 0.01
	Tumor	1.69 ± 0.42	1.67 ± 0.24	1.03 ± 0.11	n.d.
	Tumor/blood[b]	0.63	8.79	9.2	n.d.
Monomer-PEG20	Heart	9.31 ± 1.58	2.38 ± 0.32	0.99 ± 0.09	0.56 ± 0.05
	Spleen	4.61 ± 0.38	2.86 ± 0.46	2.19 ± 0.11	1.17 ± 0.11
	Kidney	46.5 ± 6.62	91.9 ± 9.14	46.7 ± 9.13	33.7 ± 2.33
	Liver	5.17 ± 0.35	3.49 ± 0.07	2.88 ± 0.20	2.27 ± 0.93
	Stomach	1.93 ± 0.3	0.75 ± 0.13	0.44 ± 0.05	0.23 ± 0.07
	Intestine	2.29 ± 0.08	1.03 ± 0.23	0.46 ± 0.05	0.21 ± 0.03
	Bone	2.18 ± 0.56	1.24 ± 0.2	0.67 ± 0.15	0.34 ± 0.08
	Blood	26.5 ± 2.85	3.93 ± 0.57	1.27 ± 0.24	0.47 ± 0.01
	Tumor	2.42 ± 0.34	9.28 ± 0.84	8.74 ± 1.33	4.85 ± 1.52
	Tumor/blood[b]	0.09	2.36	6.88	10.3
Dimer-PEG20	Heart	9.71 ± 3.53	4.64 ± 0.31	2.69 ± 0.16	1.26 ± 0.2
	Spleen	5.3 ± 0.73	3.84 ± 0.09	4.86 ± 0.97	3.01 ± 1.02
	Kidney	18.5 ± 1.24	16.7 ± 4.84	23.8 ± 2.83	13.42 ± 1.3
	Liver	6.26 ± 0.63	5.02 ± 0.33	5.95 ± 0.76	3.61 ± 0.53
	Stomach	1.89 ± 0.67	0.53 ± 0.3	0.73 ± 0.13	0.40 ± 0.23
	Intestine	2.09 ± 0.21	0.89 ± 0.18	1.01 ± 0.11	0.45 ± 0.12
	Bone	2.37 ± 0.43	1.44 ± 0.2	1.34 ± 0.09	0.64 ± 0.02
	Blood	26.3 ± 3.86	8.41 ± 0.25	5.9 ± 0.55	1.92 ± 0.07
	Tumor	2.15 ± 0.13	8.06 ± 1.73	14.9 ± 1.08	5.2 ± 0.36
	Tumor/blood[b]	0.08	0.95	2.53	2.7

[a] Not determined.
[b] The ratios represent the average of the tumor/blood values for the individual mice (n = 3) and were calculated from the non-rounded values, whereas the numbers in the table have been rounded.

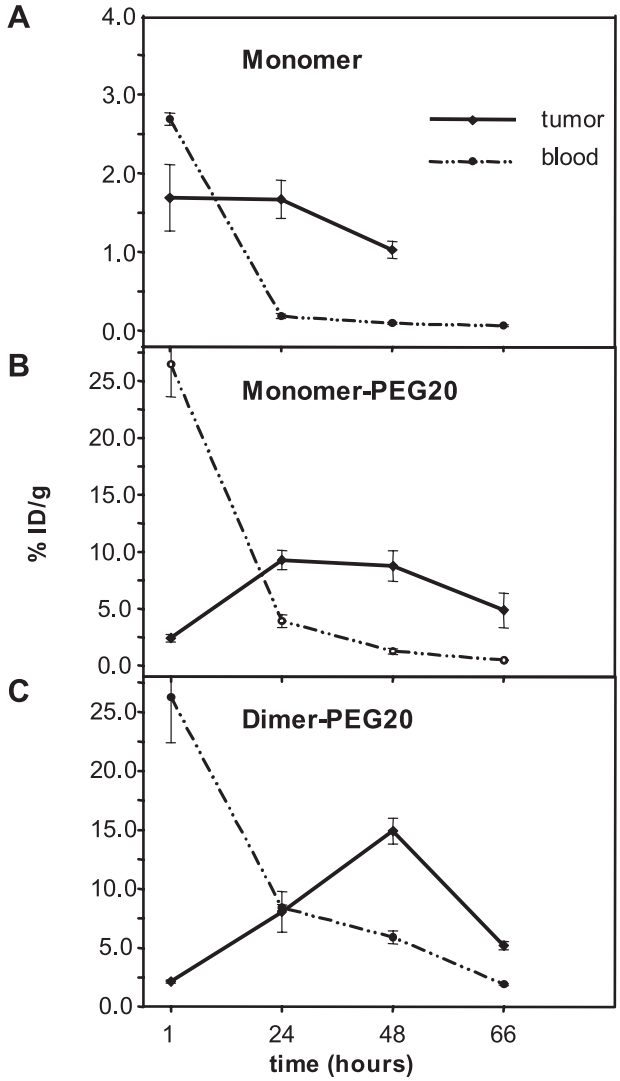

FIGURE 6. **Time-dependent changes in organ distribution of PEGylated miniantibodies compared with the scFv 4D5.** Samples of the scFv 4D5 (monomer) as well as of the PEGylated scFv (monomer-PEG20) and the PEGylated dimeric antibody fragment (dimer-PEG20) were injected into nude mice bearing SK-OV-3 carcinoma xenografts. Each mouse received 30 μg of $^{99m}Tc(CO)_3$-labeled miniantibodies intravenously. Mice ($n = 3$ per time point) were sacrificed at 1, 24, 48, and 66 h after injection, organs were excised and the incorporated radioactivity was determined. The mean % ID/g tissue ($\pm$S.D.) at each time point are given for tumor and blood. (For a detailed set of data, see Table 5.)

duced intermolecular disulfide bridges to covalently link these self-associating domains. The covalent linkage of the subunits should prevent their dissociation at high dilution over time, which otherwise might occur, when the miniantibodies are injected into the blood stream. By multimerization we not only increased the size of the 4D5 antibody fragment, but in addition its valency from a mono- to a di- up to a tetravalent construct.

In the second approach, a 20-kDa polyethylene glycol moiety (PEG20) was site-specifically linked to the C terminus of the 4D5 scFv. In contrast to the first approach, we thereby increased the molecular weight of the antibody fragment without altering its valency. This should allow us to assess the effect of molecular size on *in vivo* biodistribution independent of avidity changes. Finally, the two approaches were combined by linking the 20-kDa PEG-tail to the C termini of the dimeric miniantibody.

Molecular Characterization—The molecular characterization of the miniantibodies showed that they all could be produced in functional form and at the expected molecular composition and assembly (Figs. 2 and 3). Whereas we could not directly prove the presence of two PEG molecules on the dimer 4D5-dhlx-PEG20, the high yield of 80–90% PEGylated subunits, detected by SDS-PAGE, indicate that at least the major fraction carried a PEG-tail at both C termini. The gel filtration analysis together with dynamic light scattering (55) also revealed the strong effect of the flexible and hydrophilic PEG-tail on the hydrodynamic properties of the antibody fragments, which showed a diffusion behavior comparable to molecules with a mass of $\geq$200 kDa. This finding is in agreement with results from other groups (49, 50, 55, 68, 69).

Functional Affinities—Multimerization and PEGylation are both modifications that can alter the functional affinity of antibodies to cell surface antigens. Thus, we compared the binding behavior of the various 4D5 miniantibody formats using kinetic BIAcore measurements as well as equilibrium binding assays on human SK-OV-3 tumor cells overexpressing HER-2. On the tumor cells, all constructs showed functional affinities in the nanomolar range (Table 1), consistent with previous observations (35). In the BIAcore measurements, however, we determined functional affinities in the picomolar range (Table 2). To explain this discrepancy, one has to consider that the binding site of the antibody 4D5 is located in domain IV of the extracellular region of HER-2, which is adjacent to the transmembrane region (44) and involved in HER-2 dimerization. Thus, antibody binding to intact cells may be limited by partial inaccessibility of the target epitope. In the BIAcore measurements, however, only the extracellular domain of HER-2 was used, immobilized by its lysine residues in various positions and in random orientation.

As expected and observed in previous studies with non-covalently linked miniantibody formats (35), we found an increase in avidity by multimerization (Table 1). The magnitude of this avidity gain depends on the epitope density on the cell surface and other geometric parameters (16). PEGylation, on the other hand, led to a decrease in functional affinities of about 5-fold, both for the monomeric and the dimeric molecules, even though the attachment of the PEG-tail was site-specific at the C terminus of the proteins, most distal to the antigen binding sites. The 5-fold reduction in apparent affinity upon PEGylation of the antibody fragments was observed in the kinetic BIAcore measurements (Table 2) as well as in the equilibrium binding assays on SK-OV-3 tumor cells (Table 1). In earlier reports (69, 71, 72) it was stated that antibody conjugates with a PEG polymer attached at a single engineered cysteine distal to the antigen binding site retain full binding activity. In a more recent study (50), however, similar findings of reduced affinity as we have demonstrated here were also reported for other scFv fragments that were site-specifically conjugated with PEG polymers of different sizes.

Separate analysis of the association and dissociation kinetics revealed that the effect of PEGylation on the apparent affinity is exclusively due to decreased on-rates, while the off-rates of the

scFv or the bivalent miniantibodies barely changed upon PEGylation (Table 2). We recently investigated the reason for the decreased on-rates by experimental and computational analyses (55). A mathematical model accounting both for intra- and intermolecular blocking of the PEG-tail can robustly explain the observed binding kinetics. Briefly, careful controls could exclude that PEGylation might cause a significant percentage of permanently inactivated molecules. Rather, the flexible and bulky PEG-tail can transiently block the binding site of the antibody, decreasing the fraction of active molecules available at any given time point (intramolecular blocking). In addition, once the antibody has bound to a surface antigen (either on the cell or on a BIAcore chip), PEG may block the binding to additional neighboring antigens (intermolecular blocking). The model predicts that in solution more than 90% of the PEGylated antibodies are transiently blocked, but all molecules are intrinsically available for binding, since molecules that have bound to the target are replenished by rapid equilibration of blocked and unblocked antibodies. The model further predicts that the quantitative effect on the on-rate (and thus on affinity, as the off-rate is unchanged) is a function of antigen density on the surface (affecting intermolecular blocking) and PEG chain size (affecting both intermolecular and intramolecular blocking) (55).

Stability—Apart from a high functional affinity to the target, stability at physiological temperature and resistance to serum proteases are also crucial for effective tumor localization and retention (34). We examined the thermal stability of the different antibody constructs upon incubation in human serum at 37 °C, using gel filtration analysis as well as cell binding assays on SK-OV-3 tumor cells. We found that exposure to serum at 37 °C did not markedly change the molecular characteristics of the different antibody formats within 24 h (Fig. 4), nor did it significantly decrease their binding activity (Table 3). These results demonstrate that all 4D5 miniantibodies fulfilled the stability requirements for tumor targeting.

Tumor Targeting—The tumor targeting properties of the various 4D5 miniantibodies were analyzed in mice xenografted with human SK-OV-3 tumors. Comparing the total dose accumulation of the non-PEGylated miniantibodies, we found a moderate increase in tumor localization with increasing degree of multimerization (Table 4). These constructs showed biodistributions similar to those determined for the corresponding 4D5 miniantibodies lacking disulfide bonds between their multimerization domains (35). The covalent linkage of the multimerization domains thus did not significantly increase the serum half-life and tumor localization of the dimeric and tetrameric antibody fragments. Therefore, a potential slow dissociation of the non-disulfide-linked subunits upon the dilution that occurs after injection into the blood stream does not seem to be a major factor influencing their pharmacokinetics.

Our data (Table 4) suggest that at least the dimer 4D5-dhlx-SS is cleared by renal filtration, resulting in its rapid elimination leading in turn to reduced serum concentrations. In addition, it is likely that the multimeric proteins were more efficiently removed by macrophages, because the radioactivity associated with spleen and liver was higher than for the monomeric scFv.

Improved tumor localization has also been reported for other multimeric antibody formats (22, 23, 27, 29, 30, 36, 73) compared with their monomeric counterparts, although the use of different labeling methods, antigens and tumor types essentially precludes the direct and quantitative comparison of the data. However, what is fairly comparable to our finding is the biodistribution study of the 4D5 barnase-barstar miniantibodies (33), which only varies from our studies in the oligomerization modules used. A major difference is that because of the size of the barnase-barstar dimerization domains, the molecular weight of the whole complex is significantly larger. The favorable tumor localization of these constructs suggests that the apparent size of the molecules is a major determinant in tumor targeting, consistent with the results from PEGylation.

Although PEGylation decreased the binding affinity of the 4D5 miniantibodies, we found a clear increase in tumor accumulation (Table 5 and Figs. 5 and 6). Forty-eight hours after injection an increase in total dose accumulation of 8.5-fold for the PEGylated monomer and 14.5-fold for the PEGylated dimer was determined, each compared with the unmodified scFv at this time point. It appears that the increase in size by PEGylation had a stronger effect on tumor accumulation of the 4D5 miniantibodies than the decrease in functional affinity, which was always in the low nanomolar range. According to the tumor-to-blood ratios determined, the higher tumor enrichment seems to be mainly caused by prolonged serum half-life of the PEGylated miniantibodies. Because of the extended serum half-life and despite the high tumor accumulation, they had significantly lower tumor-to-blood ratios at earlier time points (1–24 h after injection) than the miniantibodies without a PEG-tail. Their concentration in the circulation decreased continuously but more slowly, reaching optimal tumor localization only after about 48 h. At this time point, tumor/blood ratios were >2.5. The fact that their total dose at the tumor steadily increased during the first 24–48 h indicates stable antigen binding in the tumor tissue.

Clearance Mechanisms—One reason for the prolonged serum half-life of the PEGylated miniantibodies is probably their reduced renal filtration. As shown by gel filtration analyses, the PEG moiety leads to a significant increase in hydrodynamic size of the conjugated antibody fragments, far beyond the added molecular mass, so that the resulting molecules correspond to globular proteins of $\geq$200 kDa. The tissue penetration of the miniantibodies may also be reduced by this property. Decreased extravasation into the surrounding tissue can be an additional cause of the elevated serum half-lives. Moreover, the PEG moiety may help protecting the miniantibodies from clearance by cells of the immune and reticuloendothelial system.

The higher hydrodynamic radius is reflected in lower values of kidney accumulation, which were reduced to half of that of the scFv for the scFv-PEG20 construct and to only a quarter in case of the dimeric miniantibody 4D5-dhlx-PEG20 (Table 5) (35). The observed level of radioactivity in

the kidney depends on three components, the efficiency of glomerular filtration (17, 18), reabsorption of the filtered protein in the proximal tubules (74, 75), and the retention of the radioactive label in kidney cells following protein endocytosis (76, 77).

We believe that the observed relatively high kidney values are mainly caused by the high stability of the ^{99m}Tc-label at the His tag of the proteins (56). This Tc(I) peptide complex may be unable to be transported back to the blood circulation after endocytosis and catabolism of the protein in the tubulus epithelium. Nevertheless, in contrast to other labeling methods, such as iodination, Tc(I) labeling allows a direct comparison of cellular uptake, because it more faithfully records the history of distribution of a protein. The observation that the scFv 4D5 showed an apparently reduced kidney localization when labeled with ^{125}I (56), which can be removed by dehalogenases (56, 76–78), supports this conclusion.

Besides the kidneys, the liver is a main elimination organ, usually responsible for unspecific uptake and degradation of proteins larger than 60 kDa (33, 79). Hepatic clearance appears to be responsible for elimination of the tetramer 4D5-p53-SS, when comparing its liver uptake to that of the monomeric scFv 4D5 (Table 4). On the other hand, PEGylation did not result in a significant increase in liver uptake of the antibody fragments (Tables 4 and 5). One explanation could be that the flexible PEG moiety at least partially masks the protein and its charge, thereby reducing the rate of cellular uptake. Alternatively, the PEGylated proteins may become rapidly excreted into the bile upon processing in hepatocytes and therefore do not accumulate (79).

Tumor Targeting in Comparison with other Antibody Constructs—As pointed out above, it is difficult, if not impossible, to compare tumor targeting behavior between different studies, because of the differences in models used and in experimental details. Nevertheless, we can compare trends seen within ours and other studies. Adams *et al.* (38) recently studied monomeric and dimeric scFv constructs with a C-terminal cysteine. They found a 2.5-fold increase in tumor retention when going from a monomer to a dimer and showed that this is not a MW effect but is caused by bivalent binding. In our study, the effect on tumor retention was somewhat smaller when going from the monomer to the dimer, presumably since the monomeric scFv already has a higher affinity. The *in vivo* effect of avidity will also depend on the relative position of the neighboring epitopes and the internalization of the label. The MW effect is strongly visible only at the much higher apparent molecular size caused by the addition of a PEG molecule (Tables 4 and 5). If dimerization is achieved via a bigger domain, such as a C_H3 domain (80) or a barnase-barstar pair (33), accumulation may be slightly above those with a small bivalent construct, but blood clearance is slightly slower as well. Anti-HER-2 scFvs have also been fused to the whole Fc part (39), and while anti-tumor activity was found, tumor accumulation has not been measured yet. Similarly, very large multivalent anti-HER-2 constructs have been made from Fab fragments fused in tandem (via linkers connecting the heavy chains) (40), and while their long serum half-lives have been demonstrated, their tumor accumulation was also not quantitatively assessed.

Beside quantitative tumor accumulation, immunogenicity of the antibody constructs is an important factor, determining their therapeutic applicability and efficacy. For any constructs, the ones described in the present study and others that contain artificial linker modules, potential immunogenicity is an issue. In addition, potential immunogenicity may arise from effector domains, and even fully human antibodies can elicit an immune response (81). However, the immunogenicity of protein therapeutics and their impact on anti-tumor efficacy can probably ultimately only be determined in clinical trials.

CONCLUSIONS

In vitro, the various miniantibody formats showed no obvious difference in serum stability, and thus PEGylation and oligomerization did not affect aggregation or degradation. On the other hand, they differed in serum half-life *in vivo*, suggesting that elimination by metabolism and excretion is a major determinant of their tumor targeting properties. Extended serum persistence and thereby a longer lasting reservoir of targeting molecules in the blood stream seems to be more crucial for tumor localization than increased affinity, as long as the latter is in the low nanomolar range. Therefore, out of the five tested formats, the dimeric PEGylated miniantibody 4D5-dhlx-PEG20 would be the format of choice if high tumor accumulation is desired and if long serum half-life is not a concern. For delivery of cytotoxic payloads, rapid elimination from the blood and other non-target tissues would be desired and a PEGylated scFv may best fulfill this requirement. Thus, we have demonstrated that manipulating the pharmacokinetic properties of antibodies by multimerization and PEGylation represents a valid strategy to design cancer therapeutics with tailor-made targeting properties.

Acknowledgments—We thank Christine de Pasquale for excellent technical assistance in the mouse experiments and Dr. Ilse Novak-Hofer for helpful discussions.

REFERENCES

1. Borrebaeck, C. A., and Carlsson, R. (2001) *Curr. Opin. Pharmacol.* **1,** 404–408
2. Moroney, S. E., and Plückthun, A. (2005) in *Modern Biopharmaceuticals* (Knäblein, J., ed) Vol. 3, pp. 1147–1186, Wiley-VCH, Weinheim
3. Wu, A. M., and Senter, P. D. (2005) *Nat. Biotechnol.* **23,** 1137–1146
4. Trikha, M., Yan, L., and Nakada, M. T. (2002) *Curr. Opin. Biotechnol.* **13,** 609–614
5. Weiner, L. M., and Carter, P. (2005) *Nat. Biotechnol.* **23,** 556–557
6. Adams, G. P., and Schier, R. (1999) *J. Immunol. Methods* **231,** 249–260
7. LeSauteur, L., Cheung, N. K., Lisbona, R., and Saragovi, H. U. (1996) *Nat. Biotechnol.* **14,** 1120–1122
8. Adams, G. P., Schier, R., McCall, A. M., Simmons, H. H., Horak, E. M., Alpaugh, R. K., Marks, J. D., and Weiner, L. M. (2001) *Cancer Res.* **61,** 4750–4755
9. Fujimori, K., Covell, D. G., Fletcher, J. E., and Weinstein, J. N. (1990) *J. Nucl. Med.* **31,** 1191–1198
10. Fujimori, K., Covell, D. G., Fletcher, J. E., and Weinstein, J. N. (1989) *Cancer Res.* **49,** 5656–5663

11. Graff, C. P., and Wittrup, K. D. (2003) *Cancer Res.* **63,** 1288–1296
12. Weinstein, J. N., Eger, R. R., Covell, D. G., Black, C. D., Mulshine, J., Carrasquillo, J. A., Larson, S. M., and Keenan, A. M. (1987) *Ann. N. Y. Acad. Sci.* **507,** 199–210
13. Adams, G. P., Schier, R., Marshall, K., Wolf, E. J., McCall, A. M., Marks, J. D., and Weiner, L. M. (1998) *Cancer Res.* **58,** 485–490
14. Jackson, H., Bacon, L., Pedley, R. B., Derbyshire, E., Field, A., Osbourn, J., and Allen, D. (1998) *Br. J. Cancer* **78,** 181–188
15. Rheinnecker, M., Hardt, C., Ilag, L. L., Kufer, P., Gruber, R., Hoess, A., Lupas, A., Rottenberger, C., Plückthun, A., and Pack, P. (1996) *J. Immunol.* **157,** 2989–2997
16. Plückthun, A., and Pack, P. (1997) *Immunotechnology* **3,** 83–105
17. Chang, R. L., Ueki, I. F., Troy, J. L., Deen, W. M., Robertson, C. R., and Brenner, B. M. (1975) *Biophys. J.* **15,** 887–906
18. Maack, T., Johnson, V., Kau, S. T., Figueiredo, J., and Sigulem, D. (1979) *Kidney Int.* **16,** 251–270
19. Batra, S. K., Jain, M., Wittel, U. A., Chauhan, S. C., and Colcher, D. (2002) *Curr. Opin. Biotechnol.* **13,** 603–608
20. Chester, K. A., and Hawkins, R. E. (1995) *Trends Biotechnol.* **13,** 294–300
21. Ross, J. S., Gray, K., Gray, G. S., Worland, P. J., and Rolfe, M. (2003) *Am. J. Clin. Pathol.* **119,** 472–485
22. Olafsen, T., Kenanova, V. E., Sundaresan, G., Anderson, A. L., Crow, D., Yazaki, P. J., Li, L., Press, M. F., Gambhir, S. S., Williams, L. E., Wong, J. Y., Raubitschek, A. A., Shively, J. E., and Wu, A. M. (2005) *Cancer Res.* **65,** 5907–5916
23. Hu, S., Shively, L., Raubitschek, A., Sherman, M., Williams, L. E., Wong, J. Y., Shively, J. E., and Wu, A. M. (1996) *Cancer Res.* **56,** 3055–3061
24. Carter, P., Kelley, R. F., Rodrigues, M. L., Snedecor, B., Covarrubias, M., Velligan, M. D., Wong, W. L., Rowland, A. M., Kotts, C. E., Carver, M. E., Yang, M., Bourell, J. H., Shepard, H. M., and Henner, D. (1992) *Biotechnology* (*NY*) **10,** 163–167
25. Carter, P., and Merchant, A. M. (1997) *Curr. Opin. Biotechnol.* **8,** 449–454
26. Yokota, T., Milenic, D. E., Whitlow, M., and Schlom, J. (1992) *Cancer Res.* **52,** 3402–3408
27. Werlen, R. C., Lankinen, M., Offord, R. E., Schubiger, P. A., Smith, A., and Rose, K. (1996) *Cancer Res.* **56,** 809–815
28. Viti, F., Tarli, L., Giovannoni, L., Zardi, L., and Neri, D. (1999) *Cancer Res.* **59,** 347–352
29. Huston, J. S., Adams, G. P., McCartney, J. E., Tai, M. S., Hudziak, R. M., Oppermann, H., Stafford, W. F., 3rd, Liu, S., Fand, I., Apell, G., Laminet, A. A., Houston, L. L., and Weiner, L. M. (1994) *Cell Biophys.* **24–25,** 267–278
30. King, D. J., Turner, A., Farnsworth, A. P., Adair, J. R., Owens, R. J., Pedley, R. B., Baldock, D., Proudfoot, K. A., Lawson, A. D., Beeley, N. R., Millar, K., Millican, T. A., Boyce, B. A., Antoniw, P., Mountain, A., Begent, R. H. J., Shochat, D., and Yarranton, G. T. (1994) *Cancer Res.* **54,** 6176–6185
31. Pack, P., Müller, K., Zahn, R., and Plückthun, A. (1995) *J. Mol. Biol.* **246,** 28–34
32. Le Gall, F., Kipriyanov, S. M., Moldenhauer, G., and Little, M. (1999) *FEBS Lett.* **453,** 164–168
33. Deyev, S. M., Waibel, R., Lebedenko, E. N., Schubiger, A. P., and Plückthun, A. (2003) *Nat. Biotechnol.* **21,** 1486–1492
34. Willuda, J., Honegger, A., Waibel, R., Schubiger, P. A., Stahel, R., Zangemeister-Wittke, U., and Plückthun, A. (1999) *Cancer Res.* **59,** 5758–5767
35. Willuda, J., Kubetzko, S., Waibel, R., Schubiger, P. A., Zangemeister-Wittke, U., and Plückthun, A. (2001) *J. Biol. Chem.* **276,** 14385–14392
36. Adams, G. P., Schier, R., McCall, A. M., Crawford, R. S., Wolf, E. J., Weiner, L. M., and Marks, J. D. (1998) *Br. J. Cancer* **77,** 1405–1412
37. Hudson, P. J., and Kortt, A. A. (1999) *J. Immunol. Methods* **231,** 177–189
38. Adams, G. P., Tai, M. S., McCartney, J. E., Marks, J. D., Stafford, W. F., 3rd, Houston, L. L., Huston, J. S., and Weiner, L. M. (2006) *Clin. Cancer Res.* **12,** 1599–1605
39. De Lorenzo, C., Cozzolino, R., Carpentieri, A., Pucci, P., Laccetti, P., and D'Alessio, G. (2005) *Carcinogenesis* **26,** 1890–1895
40. Miller, K., Meng, G., Liu, J., Hurst, A., Hsei, V., Wong, W. L., Ekert, R., Lawrence, D., Sherwood, S., DeForge, L., Gaudreault, J., Keller, G., Sliwkowski, M., Ashkenazi, A., and Presta, L. (2003) *J. Immunol.* **170,** 4854–4861
41. Knappik, A., and Plückthun, A. (1995) *Protein Eng.* **8,** 81–89
42. Wörn, A., and Plückthun, A. (1998) *FEBS Lett.* **427,** 357–361
43. Nahta, R., Hortobagyi, G. N., and Esteva, F. J. (2003) *Oncologist* **8,** 5–17
44. Cho, H. S., Mason, K., Ramyar, K. X., Stanley, A. M., Gabelli, S. B., Denney, D. W., Jr., and Leahy, D. J. (2003) *Nature* **421,** 756–760
45. Slamon, D. J., Clark, G. M., Wong, S. G., Levin, W. J., Ullrich, A., and McGuire, W. L. (1987) *Science* **235,** 177–182
46. Slamon, D. J., Godolphin, W., Jones, L. A., Holt, J. A., Wong, S. G., Keith, D. E., Levin, W. J., Stuart, S. G., Udove, J., and Ullrich, A. (1989) *Science* **244,** 707–712
47. Rubin, I., and Yarden, Y. (2001) *Ann. Oncol.* **12,** Suppl. 1, S3–S8
48. Bailon, P., Palleroni, A., Schaffer, C. A., Spence, C. L., Fung, W. J., Porter, J. E., Ehrlich, G. K., Pan, W., Xu, Z. X., Modi, M. W., Farid, A., Berthold, W., and Graves, M. (2001) *Bioconjug. Chem.* **12,** 195–202
49. Greenwald, R. B., Choe, Y. H., McGuire, J., and Conover, C. D. (2003) *Adv. Drug Deliv. Rev.* **55,** 217–250
50. Yang, K., Basu, A., Wang, M., Chintala, R., Hsieh, M. C., Liu, S., Hua, J., Zhang, Z., Zhou, J., Li, M., Phyu, H., Petti, G., Mendez, M., Janjua, H., Peng, P., Longley, C., Borowski, V., Mehlig, M., and Filpula, D. (2003) *Protein Eng.* **16,** 761–770
51. Cunningham-Rundles, C., Zhuo, Z., Griffith, B., and Keenan, J. (1992) *J. Immunol. Methods* **152,** 177–190
52. Hill, R. B., and deGrado, W. F. (1998) *J. Am. Chem. Soc.* **120,** 1138–1145
53. Mittl, P. R., Chene, P., and Grütter, M. G. (1998) *Acta Crystallogr. D. Biol. Crystallogr.* **54,** 86–89
54. Sowdhamini, R., Srinivasan, N., Shoichet, B., Santi, D. V., Ramakrishnan, C., and Balaram, P. (1989) *Protein Eng.* **3,** 95–103
55. Kubetzko, S., Sarkar, C. A., and Plückthun, A. (2005) *Mol. Pharmacol.* **68,** 1439–1454
56. Waibel, R., Alberto, R., Willuda, J., Finnern, R., Schibli, R., Stichelberger, A., Egli, A., Abram, U., Mach, J. P., Plückthun, A., and Schubiger, P. A. (1999) *Nat. Biotechnol.* **17,** 897–901
57. Ge, L., Knappik, A., Pack, P., Freund, C., and Plückthun, A. (1995) in *Antibody Engineering* (Borrebaeck, C. A. K., ed) pp. 229–266, Oxford University Press, Oxford
58. Bass, S., Gu, Q., and Christen, A. (1996) *J. Bacteriol.* **178,** 1154–1161
59. Schibli, R., La Bella, R., Alberto, R., Garcia-Garayoa, E., Ortner, K., Abram, U., and Schubiger, P. A. (2000) *Bioconjug. Chem.* **11,** 345–351
60. Lindmo, T., Boven, E., Cuttitta, F., Fedorko, J., and Bunn, P. A., Jr. (1984) *J. Immunol. Methods* **72,** 77–89
61. Johnsson, B., Löfas, S., and Lindquist, G. (1991) *Anal. Biochem.* **198,** 268–277
62. Myszka, D. G. (1999) *J. Mol. Recognit.* **12,** 279–284
63. Pack, P., and Plückthun, A. (1992) *Biochemistry* **31,** 1579–1584
64. Horn, U., Strittmatter, W., Krebber, A., Knüpfer, U., Kujau, M., Wenderoth, R., Müller, K., Matzku, S., Plückthun, A., and Riesenberg, D. (1996) *Appl. Microbiol. Biotechnol.* **46,** 524–532
65. Schmiedl, A., Breitling, F., Winter, C. H., Queitsch, I., and Dübel, S. (2000) *J. Immunol. Methods* **242,** 101–114
66. Ros, R., Schwesinger, F., Anselmetti, D., Kubon, M., Schäfer, R., Plückthun, A., and Tiefenauer, L. (1998) *Proc. Natl. Acad. Sci. U. S. A.* **95,** 7402–7405
67. Kadokura, H., Katzen, F., and Beckwith, J. (2003) *Annu. Rev. Biochem.* **72,** 111–135
68. Harris, J. M., and Chess, R. B. (2003) *Nat. Rev. Drug Discov.* **2,** 214–221
69. Chapman, A. P. (2002) *Adv. Drug Deliv. Rev.* **54,** 531–545
70. Kelley, R. F., O'Connell, M. P., Carter, P., Presta, L., Eigenbrot, C., Covarrubias, M., Snedecor, B., Bourell, J. H., and Vetterlein, D. (1992) *Biochemistry* **31,** 5434–5441
71. Lee, L. S., Conover, C., Shi, C., Whitlow, M., and Filpula, D. (1999) *Bioconjug. Chem.* **10,** 973–981
72. Chapman, A. P., Antoniw, P., Spitali, M., West, S., Stephens, S., and King, D. J. (1999) *Nat. Biotechnol.* **17,** 780–783
73. Casey, J. L., King, D. J., Chaplin, L. C., Haines, A. M., Pedley, R. B., Moun-

tain, A., Yarranton, G. T., and Begent, R. H. (1996) *Br. J. Cancer* **74,** 1397–1405
74. Christensen, E. I., and Birn, H. (2002) *Nat. Rev. Mol. Cell. Biol.* **3,** 256–266
75. Christensen, E. I., and Gburek, J. (2004) *Pediatr. Nephrol.* **19,** 714–721
76. Schott, M. E., Milenic, D. E., Yokota, T., Whitlow, M., Wood, J. F., Fordyce, W. A., Cheng, R. C., and Schlom, J. (1992) *Cancer Res.* **52,** 6413–6417
77. Berndorff, D., Borkowski, S., Sieger, S., Rother, A., Friebe, M., Viti, F., Hilger, C. S., Cyr, J. E., and Dinkelborg, L. M. (2005) *Clin. Cancer Res.* **11,** 7053s–7063s.
78. Kang, N., Hamilton, S., Odili, J., Wilson, G., and Kupsch, J. (2000) *Clin. Cancer Res.* **6,** 4921–4931
79. Caliceti, P., and Veronese, F. M. (2003) *Adv. Drug Deliv. Rev.* **55,** 1261–1277
80. Olafsen, T., Tan, G. J., Cheung, C. W., Yazaki, P. J., Park, J. M., Shively, J. E., Williams, L. E., Raubitschek, A. A., Press, M. F., and Wu, A. M. (2004) *Protein Eng. Des. Sel.* **17,** 315–323
81. Anderson, P. J. (2005) *Semin. Arthritis Rheum.* **34,** 19–22